Published in final edited form as:

Magn Reson Imaging. 2017 January ; 35: 29–38. doi:10.1016/j.mri.2016.08.015.

Reproducibility and Variation of Diffusion Measures in the Squirrel Monkey Brain, *In Vivo* and *Ex Vivo*

Kurt Schilling[1,2], **Yurui Gao**[1,2], **Iwona Stepniewska**[3], **Ann S Choe**[1,2], **Bennett A Landman**[2,4], and **Adam W Anderson**[1,2]

[1]Vanderbilt University Institute of Imaging Science, Vanderbilt University, Nashville, TN, USA

[2]Department of Biomedical Engineering, Vanderbilt University, Nashville, TN, USA

[3]Department of Psychology, Vanderbilt University, Nashville, TN, USA

[4]Department of Electrical Engineering, Vanderbilt University, Nashville, TN, USA

Abstract

Purpose—Animal models are needed to better understand the relationship between diffusion MRI (dMRI) and the underlying tissue microstructure. One promising model for validation studies is the common squirrel monkey, Saimiri sciureus. This study aims to determine (1) the reproducibility of *in vivo* diffusion measures both within and between subjects; (2) the agreement between *in vivo* and *ex vivo* data acquired from the same specimen and (3) normal diffusion values and their variation across brain regions.

Methods—Data were acquired from three healthy squirrel monkeys, each imaged twice *in vivo* and once *ex vivo*. Reproducibility of fractional anisotropy (FA), mean diffusivity (MD), and principal eigenvector (PEV) was assessed, and normal values were determined both in vivo and ex vivo.

Results—The calculated coefficients of variation (CVs) for both intra-subject and inter-subject MD were below 10% (low variability) while FA had a wider range of CVs, 2–14% intra-subject (moderate variability), and 3–31% inter-subject (high variability). MD in *ex vivo* tissue was lower than *in vivo* (30%–50% decrease), while FA values increased in all regions (30–39% increase). The mode of angular differences between *in vivo* and *ex vivo* PEVs was 12 degrees.

Conclusion—This study characterizes the diffusion properties of the squirrel monkey brain and serves as the groundwork for using the squirrel monkey, both *in vivo* and *ex vivo*, as a model for diffusion MRI studies.

Keywords

diffusion MRI; DTI; cortex; primate; squirrel monkey

Correspondence to: Kurt Schilling, Vanderbilt University Institute of Imaging Science, 1161 21st Avenue South, Medical Center North, AA-1105, Nashville, TN 37232-2310, USA, kurt.g.schilling@vanderbilt.edu.

Introduction

Diffusion tensor imaging (DTI) is a magnetic resonance imaging technique sensitive to the random Brownian motion of water molecules, which allows investigation of tissue microstructure. This information has also been used to perform “fiber tractography” [1, 2] in order to assess the macro-structural connectivity of the brain. Because of its noninvasiveness, DTI has become a powerful tool for *in vivo* characterization of normal and abnormal human brain white matter.

The two most common scalar quantities derived from DTI are fractional anisotropy (FA) and mean diffusivity (MD) [3]. FA is a dimensionless measure that characterizes the level of diffusion anisotropy present in a voxel, and MD is a measure of the orientationally-averaged diffusion in a voxel. Both metrics have been used extensively in human imaging studies as a means to assess and monitor various white matter diseases and disorders, including Alzheimer’s disease [4], schizophrenia [5], and multiple sclerosis [6]. Measures of MD have also found widespread use in probing the temporal evolution of stroke [7]. In addition to scalars, DTI also provides vector contrast in the form of the principal eigenvector (PEV), which is an estimate of the direction of greatest diffusivity in a voxel, and is assumed to lie parallel to the predominant axonal fiber tracts in a voxel. The PEV has been used primarily to investigate the connectivity of the brain, as it forms the basis of most fiber tractography algorithms [1].

While DTI is the only non-invasive imaging method capable of providing this information *in vivo*, *ex vivo* acquisitions are increasingly being used to probe brain connectivity and tissue properties. DTI of fixed tissue has several experimental advantages including longer scanning times and absence of motion. Together, this makes it possible to obtain data with high signal-to-noise ratio (SNR) at a much higher resolution compared to *in vivo* studies, allowing visualization of more intricate fiber structures. Because of these advantages, there has been an increasing number of diffusion MRI studies on the fixed, *ex vivo* brain.

Another advantage afforded by *ex vivo* diffusion MRI is the ability to compare diffusion data directly to histological data. This is particularly useful in validation studies that aim to determine the biological basis of diffusion contrast, as well as hodological studies testing the legitimacy of diffusion MRI tractography measures. A major problem in validation studies in humans, however, is that there is no histological gold standard available. It is difficult to obtain high quality fixed human brain tissue, as perfusion fixation is not a viable option and immersion fixation typically cannot be performed in a timely manner, hence the need for animal models. One promising model for validation studies is the common squirrel monkey, Saimiri sciureus. The functional and microstructural organization of the central nervous system of the squirrel monkey is similar to that of humans [8, 9], making this species a commonly-used non-human primate model in biomedical research [10]. The small brain of the squirrel monkey is also easy to process histologically. However, the *in vivo* and *ex vivo* diffusion properties of the squirrel monkey brain have not been thoroughly investigated. Thus, the purpose of this study is to characterize the diffusion properties of the common squirrel monkey brain *in vivo* and *ex vivo*, and determine the extent to which *ex vivo* diffusion measurements reflect the corresponding *in vivo* values.

To do this, several issues need to be considered. First, it is essential to assess the reproducibility of diffusion measures in the squirrel monkey. Because quantitative comparisons, both between and within subjects over time, rely on accurate and reliable measurements, it is necessary to characterize the limitations of these measurements. Here, we repeat reproducibility studies performed on human *in vivo* diffusion data [11, 12] in order to establish measurement reliability in the squirrel monkey brain. Similarly, it is important to determine normal diffusion values in the squirrel monkey brain, not only to establish standards for the healthy brain, but also to demonstrate that diffusion in the squirrel monkey brain is representative of that in the human brain. Finally, it should be established how well the *ex vivo* properties reflect those of the living monkey brain. Several groups have compared *in vivo* and aldehyde-fixed *ex vivo* data in order to aid in interpreting DTI of the fixed brain [13–15], and we repeat these studies for the first time on the squirrel monkey brain.

Therefore, the goals of this study are threefold: (1) to measure the reproducibility of *in vivo* DTI measures both within and between subjects, (2) to evaluate the agreement between *in vivo* and *ex vivo* DTI data acquired from the same specimen, and (3) to determine the normal values and their variation in white matter (WM) and gray matter (GM) regions of interest (ROIs). Together, this study serves to characterize the diffuson MRI properties of the squirrel monkey brain, both in vivo and ex vivo, and serves as a valuable resource for future diffusion MRI studies that choose to utilize this animal model.

Methods

The data used here were acquired as part of a larger project, which aims to create the first combined histological and MRI atlas of the squirrel monkey brain [16]. Briefly, each monkey brain was imaged in three scan sessions, twice *in vivo* and once *ex vivo*. The brain was then sectioned and stained in order to facilitate expert labeling of anatomical ROIs. All animal procedures for this study were approved by the Vanderbilt University Animal Care and Use Committee, and followed guidelines of National Institutes of Health for the care and use of laboratory animals. The monkey was housed in adjoining individual primate cages allowing social interactions with other monkeys and received extensive environmental enrichment such as play objects that are changed for variability, novel food objects and foraging devices. Normal food, treats and fruit were provided to the animal by trained staff. Analgesics were given following the procedure and in response to any evidence of pain (behavioral abnormality, loss of appetite, tissue edema, or muscle spasms). The monkey was closely monitored in the week following the surgical procedures. All MRI scans were performed on the same 9.4T Agilent scanner, and the same process was performed on three squirrel monkeys (Saimiri sciureus). The monkeys were young adults (3, 4, and 5 years old and weighed 838g, 770g, and 616g, respectively, at the time of the first scan session).

In vivo MRI data acquisition

The two *in vivo* sessions were separated by a 20-day interval. During each in vivo session, the live squirrel monkey was anaesthetized and the brain was scanned with a standard T1-weighted gradient echo multi-slice (GEMS) sequence (TR = 404ms, TE = 2.4ms, flip angle

= 20°, 630μm isotropic voxels, 64×64×80 matrix), followed by diffusion weighted imaging using a pulsed gradient spin echo (PGSE) echo planar imaging (EPI) sequence (TR=5.5s, TE=44ms, 32 gradient directions, 630um isotropic voxel, 64×64×65 matrix). The nominal b-factor was 1000s/mm^2, but this was corrected for cross-terms involving imaging gradients, on a per-direction basis.

Ex vivo MRI data acquisition

Four weeks after the second *in vivo* scan, the monkey was given a lethal dose of barbiturate, and perfused through the heart. All blood was rinsed out with physiological saline (0.9% NaCl) followed by fixative (4% paraformaldehyde). The brain was removed from the skull and stored in buffered saline overnight. Then the brain was scanned with a GEMS sequence with full brain coverage (TR = 963ms, TE = 4ms, flip angle = 20°, 300μm isotropic voxel, 192×128×115 matrix). Diffusion weighted scans were performed using a PGSE multi-shot spinwarp imaging sequence with the same FOV as the structural images (TR=4.6s, TE=42ms, 32 gradient directions, b ≈1000s/mm^2, 300μm voxel, 192×128×115 matrix). Acquisition for a single diffusion-weighted volume took approximately 10 minutes. Due to hardware limitations, the b-factor used in this experiment is lower than the optimum b-value for DTI in fixed brain based on the expected diffusivity [13]. To compensate for the decreased contrast-to-noise ratio caused by the low b-value, the scan time was extended to 50 hours (9 averages), which yielded a contrast-to-noise ratio comparable to *in vivo* human studies (e.g., a human *in vivo* study with MD = 0.7E-3 mm^2/s and SNR=20). One subject's ex vivo scan was found to be corrupted, and was not included in the following analysis.

Data processing

All DTI processing was performed in the coordinate system the data were acquired in. Steps included correction for motion/eddy current distortion by affine registration of each diffusion-weighted volume to the non-diffusion weighted volume, correction of gradient tables, and log-linear tensor fitting. Fractional anisotropy, MD, PEVs, and diffusion-encoded color-maps were computed for all diffusion data sets (Figure 1).

In order to perform comparisons both within and between monkeys, it is convenient to align all data to a "common space". From the non-diffusion weighted volumes (b0 volumes) of all datasets, a standard-space template was created using an iterative registration procedure similar to that used for templates of the human brain [17]. Next, the non-diffusion weighted volumes were registered to the template using linear and nonlinear registration implemented in FSL [18]. By applying the resulting deformation fields, all tensors, FA maps, MD maps, PEVs, and color-maps were transformed to the common space. The tensor, eigenvectors, and color-maps were then re-oriented using the preservation of principal directions strategy [19]. Figure 2a provides an overview of the data processing procedures.

To assess the accuracy of registration to the template, a surface-based distance metric [20] was calculated for each b0 volume after registration to the template. A surface mask of the template was created using an intensity threshold. Surface masks were also created for all b0 images in native space and transformed into common space by applying the deformation fields obtained from the aforementioned procedures. For every surface voxel of the template,

the Euclidean distance to the nearest surface voxel of each transformed b0 image was calculated.

All processing steps, including registrations, transformations, and visualization were performed with the MIPAV (Medical Image Processing, Analysis, and Visualization) [21] software package and FSL FLIRT/FNIRT (FMRIB's Image Registration Tools) [18].

ROI definition: block and micrograph acquisition

In order to obtain ground truth WM and GM parcellations, we choose to define all ROIs on histological samples and register these parcels to MRI data of the same monkey. Following MRI scanning, the brain was frozen and cut serially on a microtome in the coronal plane at 50 um thickness. The surface of the frozen tissue block (i.e., the "block-face") was photographed using a Canon digital camera (image resolution = 50um/pixel, image size = 3330*4000 pixels, number of images per brain ~200) prior to cutting every third section (i.e., at 150 um intervals). These block-face images have been shown to produce more robust inter-modality registration results by providing a relatively undistorted intermediate reference space between the histological and MRI data [22].

Every sixth section was stained for Nissl substance in order to identify the borders of the cortical ROIs based on their cytoarchitectural features [23]. Adjacent series were stained for myelin using Gallyas silver stain [24] for identification of WM ROIs. All sections were photographed under 0.5x magnification using a Nikon DXM1200F digital camera mounted on a Nikon E-800 microscope (image resolution = 7um/pixel). Eighteen cortical GM ROIs and 5 WM tracts were labeled by an expert using the Nissl-stained and myelin-stained micrographs and were digitized.

ROI definition: micrograph to DTI-space registration

The digitized ROIs were registered to the DTI image data using a multi-step registration procedure [25]. First, every histological section was downsampled and registered to the downsampled photograph of the corresponding tissue block using mutual information based 2D linear registration followed by 2D nonlinear registration using the adaptive bases algorithm (ABA) [26]. Next, all down-sampled block photographs were assembled into a 3D block volume, which was then registered to the *ex vivo* DTI volume using a 3D affine transformation followed by 3D nonlinear registration with ABA. The deformation fields produced above could be applied to the 2D digitized ROIs to transfer these regions into DTI native space. Using the deformation fields described in the "Data Processing" section above, these ROIs were then aligned to the common space. An overview of the ROI creation and registration procedures is shown in Figure 2b.

Quantitative analysis

To assess the reproducibility of the *in vivo* scan sessions, the percent coefficient of variation (CV) was calculated for FA and MD for all ROIs. The CV is the most commonly reported measure of relative reproducibility in the literature and simply represents the dispersion of the data. The intra-subject CV was calculated by taking the standard deviation of a measure of interest (FA or MD) in a particular ROI and dividing this quantity by the mean for the

particular ROI. The inter-subject CV was calculated by taking the standard deviation of a measure across animals and dividing by the mean across subjects [27, 28]. For variables related to biomedical imaging, CVs below 10% are considered desirable and indicate a small amount of variability in the dependent variable. Coefficients of variation between 11% and 20% indicate a moderate amount of variability, and greater that 21% are considered highly variable [12].

Comparison of *in vivo* and *ex vivo* DTI was performed in the common space. Fractional Anisotropy and MD were analyzed using an ROI based approach, while the angular difference in PEV was computed voxel-wise.

The ROIs were also examined in the non-diffusion weighted images in order to determine the SNR [29]. All statistical calculations were performed using custom routines written in MATLAB.

Results

Common space and ROI definition

The average registration quality over all data sets is displayed over the surface of the template in Figure 3a. The surfaces of the volumes tend to align well, with most areas accurate to within the size of the *in vivo* MRI voxel (630um). Outliers appear in the most anterior parts of the prefrontal cortex, in the visual cortex, and a large area involving motor and somatosensory areas.

For all monkeys, the digitized ROIs labeled in the light microscopy datasets were registered to their respective *ex vivo* DTI volumes, and finally to the common space. Minor manual edits were performed to ensure continuity of the ROIs. Three-dimensional renderings of the 18 GM and 5 WM ROIs of one monkey are shown in Figure 3b.

Reproducibility of *in vivo* scans

The SNR, mean ROI values, intra-subject CV and inter-subject CV for FA and MD are shown in Table 1. Intra-subject variation for MD ranges between 0.30% and 6.87% for all ROIs, while that of FA ranges between 4.8% and 16.8% for GM ROIs and from 1.5% to 8.4% for WM ROIs. Inter-subject variation ranged between 0.4% to 7.4% for MD and between 3.4% and 31.6% for FA. Regions that had highly variable FA (greater than 20%) included left and right primary motor area (M1), right and left supplementary motor area (SMA), left anterior (PAC) and posterior parietal (PPC) areas, and left premotor area (PM).

From table 1, three trends are apparent. First, with a few exceptions, the intra-subject FA variation is less than the inter-subject variation. Second, the MD exhibits a lower CV than the corresponding FA CV for all ROIs. And finally, the WM variation tends to be less than GM variation.

The angular difference in orientations of the PEVs between the first and second *in vivo* scan sessions was calculated for each WM voxel. Typical results from one monkey are shown in

histogram form in Figure 4a. The histogram shows a peak angular difference of 5 degrees, an average deviation at 12 degrees, and over 75% of voxels agreeing to within 15 degrees.

In vivo and *ex vivo* comparisons

Typical results for comparison of *in vivo* and *ex vivo* DTI values for one monkey are shown in Figure 4b–d. First, the angular difference between the in vivo PEV and ex vivo PEV for all WM voxels of the same monkey are displayed in Figure 4b. There is a notable increase in the angular difference, as opposed to the comparison of the two *in vivo* scans (Figure 4a). The histogram peaks at an angular difference of 12 degrees, and the two scans have a mean angular difference of 22 degrees. Over 75% of voxels agree to within 25 degrees.

Figure 4c displays the MD across all ROIs for both *in vivo* scans (blue) and the *ex vivo* scan (red). MD in the fixed *ex vivo* tissue is much lower than those of the living monkey, showing decreases between 30% and 50% from that of the *in vivo* diffusivity. The averaged MD (in units of 10^{-4} mm^2/s) for the whole brain, all GM, and all WM are 7.40, 7.53, and 7.13, respectively, for the *in vivo* scans, and 4.88, 5.01, and 4.50, respectively, for the *ex vivo* scans.

The results from a similar analysis of FA are shown in Figure 4d. On average, WM FA was 139+/−21% of *in vivo* values in the fixed brain. Corresponding values in GM were 130+/−17%. A regression analysis of FA values for all ROIs of the *in vivo* versus fixed brain showed a significant model II correlation with a slope of .73 ($r=.75$, $p<.01$).

Discussion

Reproducibility of *in vivo* diffusion scans

The first aim of this study was to investigate within-monkey and between-monkeys variability of three different DTI measurements in the squirrel monkey brain. Characterizing the regional variation of these diffusion MRI measurements is critical for interpreting results of longitudinal studies and group comparisons. Various groups have assessed the variability of DTI measures in human brain [12, 30–33]; however, this analysis has not been performed on the squirrel monkey brain. Here, we quantified the reproducibility of the FA and MD by calculation of an ROI-based CV, as well as determined the voxel-wise agreement of the primary eigenvector orientation.

We find that the variation in diffusion measures in the squirrel monkey brain is on par with that of the human, as the CVs reported here for ROIs align well with studies of the human brain [12, 30, 34, 35]. In agreement with our results, the literature tends to support higher inter-subject variability than intra-subject, larger CVs in GM than in WM, and CVs for MD lower than those of FA. Papinutto et al. [35] reported most between-session intra-subject CV values between 1% and 4% for MD and 2% and 6% for FA; however, their analysis was restricted to 3 ROIs. Using a 3*3 ROI mask, Heiervang et al. [30] reported inter-session CVs below 3% and inter-subject CVs below 8% for MD.. Our methods most closely replicate the analysis of Marenco et al. [12], with 2 scans per subject, registered to a standard space template, and analysis performed on both WM and GM ROIs. In their study, within-subject CV was reported to be between 3–21% for FA WM and GM, and between 2–8% for MD

WM and GM. Finally, Heim et al. [34] derived measures related to intra-session reproducibility using bootstrapping techniques to assess FA measures. The authors calculated CVs for FA in GM to be 25±1% and 15±1% in WM, again, consistent with our inter-session findings of CVs for MD lower than for FA.

The outliers in the inter-subject FA measures can likely be explained by poor registration of one or more scan sessions. Many of these regions coincide with the area on the left hemisphere where registration errors were most prominent (Figure 3a), specifically part of PM, M1, and smaller areas of PAC and PPC. Also, registration errors are seen in the most anterior and most posterior regions of the brain, corresponding to the prefrontal cortex (PFC) and part of primary visual cortex (V1), respectively. In addition, it is expected on theoretical grounds [36, 37] that MD is more robust to noise than is FA, and the effects of noise on FA decrease with increasing anisotropy (i.e., the CV of FA is expected to be larger in GM than in WM). However, the reproducibility of DTI-derived MD and FA in the squirrel monkey brain is consistent with that of *in vivo* human scans.

Previous studies [38, 39] have shown that diffusion weighted schemes with a low number of unique directions can cause bias and variability in the orientation of the PEV. In our study, we use a 32-direction diffusion weighted scheme, and find a mean angular difference between two *in vivo* sessions to be 12 degrees over all WM. In an *in vivo* human study on the effects of SNR on the reproducibility of the PEV across sessions, Farrel et al. [33] described angular deviations as high as 20 degrees in WM regions, with mean angular deviations ranging from 6 to 12 degrees across ROIs. Thus, in addition to MD and FA, the PEV reproducibility is consistent with human studies.

Comparison of *in vivo* and *ex vivo* diffusion properties

Comparisons between *in vivo* and fixed brains have been performed in rodents [14, 15, 40, 41], macaques [13, 42], and in humans [43, 44]; however, similar analysis has not been performed in the squirrel monkey brain. In addition, this study is unique in that a direct comparison of the same specimen is made both *in vivo* and *ex vivo*. Our results show a significant increase in FA in the fixed *ex vivo* squirrel monkey brain, with a greater increase in WM than in GM. Some studies [13, 40] have demonstrated the maintenance of diffusion anisotropy after excision and fixation of the tissue, however others [42, 44] have shown a decreased FA *ex vivo*. The discrepancy is likely caused by the differences in fixation method, postmortem intervals (the time between death and tissue fixation), and scan interval (time from death to scan). Once fresh tissue is removed from the body, it begins a process of self-destruction or autolysis, which will continue until the tissue is fixed [45]. Because of this, pronounced decreases in anisotropy have been observed the longer fixation is delayed [41]. The tissues in this study were perfusion fixed and scanned within 24 hours, meaning the postmortem interval and scan interval are minimized, whereas studies in humans cannot be perfusion fixed, and are typically immersion fixed days after death [14, 44].

Furthermore, the smaller voxel size of the *ex vivo* scans could account for higher FA in fixed tissue. A higher resolution will reduce the partial volume effects from different tissue types, as well as reduce the occurrence of multiple fiber orientations within a voxel. Both effects are expected to increase the observed anisotropy [46]. It is important to note that in the high

resolution *ex vivo* scans, we are able to observe diffusion anisotropy in the cortex, which is known to have coherently aligned microstructure. This phenomenon has also been described in the human cortex [44]. Our studies best align with that of D'Arceuil et al. [13] performed in the macaque brain, where they noted a slight but consistent increase in FA in both postmortem fresh and postmortem fixed brains.

It is well known that diffusivity in the brain declines significantly at death. This effect is partially attributed to the reduced tissue temperature (~38 °C *in vivo*; ~20 °C *ex vivo* in our study), along with the effects of formalin fixation including protein cross-linking, dehydration, tissue degradation [47, 48], and decreased membrane permeability [49]. Our results show that the fixed squirrel monkey brain MD declines by 34±5% of the *in vivo* value over all regions of interest, with a decline of 33±4% in GM ROIs and 38±5% in WM ROIs. Previous comparisons of *in vivo* and *ex vivo* diffusion properties in macaque brain show decreases between 30–50% in fresh *ex vivo* brains, and between 50 and 80% in fixed brains [13, 42]. Again, the discrepancy is likely due to the degree of tissue degeneration post mortem, and differences due to perfusion versus immersion fixation.

Our results indicate that the PEV reproducibility between *in vivo* and *ex vivo* scans is less than that between multiple *in vivo* sessions. The observed PEV has been shown to be sensitive to SNR [33], diffusion weighting schemes [32], and partial volume or resolution effects. In our study, the average SNR for *ex vivo* GM and WM is 21 and 15, respectively, while the same for *in vivo* is 32 and 21. The reproducibility of the PEV orientation will likely improve with an increased SNR [32]. Most importantly, DTI does not adequately resolve crossing fibers. Because of the larger voxel size, the *in vivo* acquisition is much more susceptible to the crossing and bending fiber effects, and will produce an "orientationally averaged" PEV that may not correspond to the true direction of any fibers in the voxel. To gain a better understanding of where the PEV fails to be reproducible, we chose to visualize the PEVs in both *in vivo* and *ex vivo* scans simultaneously, with the *in vivo* PEVs up-sampled to the *ex vivo* resolution. Figure 5 shows an FA map in the coronal plane, overlaid with the *in vivo* and *ex vivo* PEV's displayed as "sticks" (*ex vivo*, red; *in vivo*, blue). It is easy to see agreement in areas of high anisotropy (i.e. corpus callosum and corticospinal tract), but in regions of crossing and bending fibers the *in vivo* and *ex vivo* PEVs can be nearly perpendicular to each other. The widespread agreement in orientation estimations, as well as the existence of diffusion anisotropy *ex vivo*, suggest that the tissue microstructures that influence diffusion *in vivo* is largely the same after fixation, which lends support to the use of *ex vivo* DTI as a means to validate the contrast seen *in vivo*.

The differences in FA and PEV between *in vivo* and *ex vivo* scans have important implications for fiber tractography. Using similar *in vivo* and *ex vivo* acquisitions, Gao et al. [50] performed deterministic fiber tracking and described much shorter fibers *in vivo*, as well as a lower *in vivo* correlation to known WM fiber pathways. These results are expected, due to a combination of a lower resolution and decreased FA, which causes early termination when the stopping criterion is based on an FA threshold.

Normal diffusion values

Because myelin density, cell density, and cell size vary across the squirrel monkey cortex [51], it is reasonable to expect simple DTI measures like FA and MD to vary as well. The third aim of this study is to determine the normal diffusion values and their distribution throughout the brain. This is necessary as a prerequisite for neuroscience research, not only as a means to characterize tissue microstructure and integrity in the healthy squirrel monkey brain, but also to relate and extrapolate the results from the squirrel monkey brain to those of the human brain.

As shown in table 1, the average MD for *in vivo* GM ROIs ranged from 7.02 to 8.25 [10^{-4} mm^2/s], and from 7.13 to 7.89 for WM ROIs. *Ex vivo*, the average MD for GM ROIs ranged from 4.91 to 5.39, and from 4.26 to 4.84 for WM ROIs (not shown). For FA, *in vivo* ROIs ranged from an average of 0.17 to 0.23 for GM, and 0.38 to 0.70 in WM. *Ex vivo* ROIs had an average FA ranging from 0.19 to 0.25 in GM, and 0.52 to 0.86 in WM.

Since the early days of DTI, it was recognized the MD is fairly homogenous in the normal brain parenchyma, with remarkably low interspecies variability [52]. Normal human diffusivity values have been measured in the range 6.9–10.1 mm^2/s [52–56], with slightly lower diffusivities in WM than in GM. This range reported between studies may seem surprisingly large, however, low variability of MD is reported within studies, as is the case in this study. Variation across studies may originate from various acquisition parameters, including b-value, diffusion times, and size of ROI's [57]. Large variations in FA have also been reported in the literature. Gray matter (both cortical and subcortical) FA has been measured in the range of 0.05 to 0.25 [12, 53], while that of WM regions can vary considerably based on the tract, and even within the tract itself. For example, one of the most easily identifiable and highly anisotropic regions, the corpus callosum, has been reported to vary between 0.7 [11] and 0.89 [55], and shows variation between the different regions of the tract itself (i.e. genu vs. splenium) [12, 55]. Based on the results of this study, we can conclude that the *in vivo* diffusion measures of the squirrel monkey brain are similar to those of the human brain, showing that the squirrel monkey is indeed a valid model for diffusion MRI studies.

In addition to the ROI-based approach, we also visualized the voxel-wise distribution of MD and FA throughout the cortex of both the *ex vivo* and *in vivo* squirrel monkey brain in Figure 6. Again, the significant drop in *ex vivo* diffusivity (Figure 6b) compared to *in vivo* (Figure 6d) is apparent. These renderings also suggest much less variation of diffusivity in the *ex vivo* cortex, consistent with the ROI-based findings. Interestingly, the *ex vivo* squirrel monkey brain shows a slightly increased MD near the PM, M1, and SMA regions (light blue in Figure 6b), while the *in vivo* rendering shows decreased diffusivity in the PF and V1 cortical regions (yellow, Figure 6d). These observations correlate well with the known cell densities across the squirrel monkey cortex [51], with M1 and PM having the lowest cell and neuron densities, while the V1 and extrastriate cortical areas have the highest densities. Consistent with the ROI analysis, the *ex vivo* FA is consistently higher than *in vivo*. Also, both show similar trends of increased FA in the PFC, as well as the APC and PPC cortical area, a region which has relatively high cell densities, as well as a very distinct cortical layer (layer 4) consisting of small, aligned granular cells, which could contribute to the increased

FA. While only a qualitative analysis, these results suggests that, as in humans, DTI is sensitive to the underlying tissue microstructure of the squirrel monkey brain. However, further studies are necessary to determine the relative contributions of cell size, cell density, and myelin content to DTI measures.

Limitations

A limitation to this study is potential residual misalignment between ROIs identified through histology and the DTI data. Registration errors could introduce partial volume effects between different regions, as well as different tissue types, which could amplify calculated CVs. The registration pipeline used in this study has been shown to be accurate to approximately 300um (the size of our imaging voxels), using data of comparable resolution and quality [25]. While ROIs on human data are typically identified directly on the MRI images [12, 30, 35], we chose to exploit subsequent histology to create cytoarchitecture and microarchitecture-informed ROIs. This allows a parcellation scheme that includes regions that could not have been identified using MRI alone. Related to this, the use histologically-derived ROIs has limited our analysis to three subjects. It is possible to use the DTI data itself to develop a tractography-based approach to segment WM and GM structures of interest [58–60], however, the accuracy and reliability of these techniques with respect to the histological gold standard has not been established.

Conclusion

In this work, we have characterized the diffusion properties of the squirrel monkey brain. First, We find that the reproducibility of the MD, FA, and PEV is comparable to that of human DTI studies, establishing the validity of quantitative cross-sectional and longitudinal DTI studies on the squirrel monkey. Second, the relationship between *in vivo* and *ex vivo* measurements is considered. We confirm that death and fixation causes significant changes to diffusion MRI metrics, specifically a decreased MD and (in our case) an increased FA. However, care must be taken in correlating diffusion measures from *ex vivo* brains due to differences in postmortem intervals and scan intervals. Finally, we provide the normal values of diffusion indices in a variety of both white and gray matter regions of interest. This study is the first to address these issues in the squirrel monkey brain. Thus, it serves as the basis for using the squirrel monkey for diffusion MRI studies, and supports the use of *ex vivo* DTI, as well as subsequent histology, as a means of understanding image contrast seen on *in vivo* scans.

Acknowledgments

This research was supported by National Institutes of Health grants 2R01-NS58639, and 1S10 RR 17789.

References

1. Mori S, van Zijl PCM. Fiber tracking: principles and strategies – a technical review. NMR in Biomedicine. 2002; 15(7–8):468–480. [PubMed: 12489096]
2. Mori S, Crain BJ, Chacko VP, van Zijl PC. Three-dimensional tracking of axonal projections in the brain by magnetic resonance imaging. Ann Neurol. 1999; 45(2):265–9. [PubMed: 9989633]

3. Basser PJ, Pierpaoli C. Microstructural and physiological features of tissues elucidated by quantitative-diffusion-tensor MRI. J Magn Reson B. 1996; 111(3):209–19. [PubMed: 8661285]
4. Takahashi S, Yonezawa H, Takahashi J, Kudo M, Inoue T, Tohgi H. Selective reduction of diffusion anisotropy in white matter of Alzheimer disease brains measured by 3. 0 Tesla magnetic resonance imaging. Neurosci Lett. 2002; 332(1):45–8. [PubMed: 12377381]
5. Kubicki M, Shenton ME. Diffusion Tensor Imaging findings and their implications in schizophrenia. Curr Opin Psychiatry. 2014; 27(3):179–84. [PubMed: 24613986]
6. Filippi M, Cercignani M, Inglese M, Horsfield MA, Comi G. Diffusion tensor magnetic resonance imaging in multiple sclerosis. Neurology. 2001; 56(3):304–11. [PubMed: 11171893]
7. Ulug AM, Beauchamp N Jr, Bryan RN, van Zijl PC. Absolute quantitation of diffusion constants in human stroke. Stroke. 1997; 28(3):483–90. [PubMed: 9056600]
8. Nudo RJ, Sutherland DP, Masterton RB. Variation and evolution of mammalian corticospinal somata with special reference to primates. The Journal of Comparative Neurology. 1995; 358(2):181–205. [PubMed: 7560281]
9. Heffner RS, Masterton RB. The Role of the Corticospinal Tract in the Evolution of Human Digital Dexterity. Brain, Behavior and Evolution. 1983; 23(3–4):165–183.
10. Abee CR. The Squirrel Monkey in Biomedical Research. ILAR Journal. 1989; 31(1):11–20.
11. Pfefferbaum A, Adalsteinsson E, Sullivan EV. Replicability of diffusion tensor imaging measurements of fractional anisotropy and trace in brain. J Magn Reson Imaging. 2003; 18(4): 427–33. [PubMed: 14508779]
12. Marenco S, Rawlings R, Rohde GK, Barnett AS, Honea RA, Pierpaoli C, Weinberger DR. Regional distribution of measurement error in diffusion tensor imaging. Psychiatry Res. 2006; 147(1):69–78. [PubMed: 16797169]
13. D'Arceuil HE, Westmoreland S, de Crespigny AJ. An approach to high resolution diffusion tensor imaging in fixed primate brain. Neuroimage. 2007; 35(2):553–65. [PubMed: 17292630]
14. Guilfoyle DN, Helpern JA, Lim KO. Diffusion tensor imaging in fixed brain tissue at 7. 0 T. NMR Biomed. 2003; 16(2):77–81. [PubMed: 12730948]
15. Sun SW, Neil JJ, Song SK. Relative indices of water diffusion anisotropy are equivalent in live and formalin-fixed mouse brains. Magn Reson Med. 2003; 50(4):743–8. [PubMed: 14523960]
16. Gao Y, Khare SP, Panda S, Choe AS, Stepniewska I, Li X, Ding Z, Anderson A, Landman BA. A brain MRI atlas of the common squirrel monkey. Proc Soc Photo Opt Instrum Eng. 2014; 9038:90380c.
17. Fonov V, Evans AC, Botteron K, Almli CR, McKinstry RC, Collins DL. Unbiased average age-appropriate atlases for pediatric studies. NeuroImage. 2011; 54(1):313–327. [PubMed: 20656036]
18. Smith SM, Jenkinson M, Woolrich MW, Beckmann CF, Behrens TE, Johansen-Berg H, Bannister PR, De Luca M, Drobnjak I, Flitney DE, et al. Advances in functional and structural MR image analysis and implementation as FSL. Neuroimage. 2004; 23(Suppl 1):S208–19. [PubMed: 15501092]
19. Alexander DC, Pierpaoli C, Basser PJ, Gee JC. Spatial transformations of diffusion tensor magnetic resonance images. Medical Imaging, IEEE Transactions on. 2001; 20(11):1131–1139.
20. Jiang H, Robb RA, Holton Tainter KS. New approach to 3-D registration of multimodality medical images by surface matching. 1992:196–213.
21. McAuliffe MJ, Lalonde FM, McGarry D, Gandler W, Csaky K, Trus BL. Medical Image Processing. Analysis and Visualization in clinical research. 2001:381–386.
22. Toga AW, Ambach KL, Schluender S. High-resolution anatomy from in situ human brain. Neuroimage. 1994; 1(4):334–44. [PubMed: 9343583]
23. Preuss TM, Stepniewska I, Kaas JH. Movement representation in the dorsal and ventral premotor areas of owl monkeys: a microstimulation study. J Comp Neurol. 1996; 371(4):649–76. [PubMed: 8841916]
24. Gallyas F. Silver staining of Alzheimer's neurofibrillary changes by means of physical development. Acta Morphol Acad Sci Hung. 1971; 19:1–8. [PubMed: 4107507]

25. Choe AS, Gao Y, Li X, Compton KB, Stepniewska I, Anderson AW. Accuracy of image registration between MRI and light microscopy in the ex vivo brain. Magn Reson Imaging. 2011; 29(5):683–92. [PubMed: 21546191]
26. Rohde GK, Aldroubi A, Dawant BM. The adaptive bases algorithm for intensity-based nonrigid image registration. IEEE Trans Med Imaging. 2003; 22(11):1470–9. [PubMed: 14606680]
27. Bland JM, Altman DG. Measurement error. Bmj. 1996; 313(7059):744. [PubMed: 8819450]
28. Bland JM, Altman DG. Measurement error proportional to the mean. Bmj. 1996; 313(7049):106. [PubMed: 8688716]
29. Carlson HL, Laliberte C, Brooks BL, Hodge J, Kirton A, Bello-Espinosa L, Hader W, Sherman EM. Reliability and variability of diffusion tensor imaging (DTI) tractography in pediatric epilepsy. Epilepsy Behav. 2014; 37c:116–122.
30. Edelstein WA, Bottomley PA, Pfeifer LM. A signal-to-noise calibration procedure for NMR imaging systems. Medical Physics. 1984; 11(2):180–185. [PubMed: 6727793]
31. Heiervang E, Behrens TE, Mackay CE, Robson MD, Johansen-Berg H. Between session reproducibility and between subject variability of diffusion MR and tractography measures. Neuroimage. 2006; 33(3):867–77. [PubMed: 17000119]
32. Landman BA, Farrell JA, Jones CK, Smith SA, Prince JL, Mori S. Effects of diffusion weighting schemes on the reproducibility of DTI-derived fractional anisotropy, mean diffusivity, and principal eigenvector measurements at 1. 5T. Neuroimage. 2007; 36(4):1123–38. [PubMed: 17532649]
33. Farrell JA, Landman BA, Jones CK, Smith SA, Prince JL, van Zijl PC, Mori S. Effects of signal-to-noise ratio on the accuracy and reproducibility of diffusion tensor imaging-derived fractional anisotropy, mean diffusivity, and principal eigenvector measurements at 1. 5 T. J Magn Reson Imaging. 2007; 26(3):756–67. [PubMed: 17729339]
34. Papinutto ND, Maule F, Jovicich J. Reproducibility and biases in high field brain diffusion MRI: An evaluation of acquisition and analysis variables. Magn Reson Imaging. 2013; 31(6):827–39. [PubMed: 23623031]
35. Heim S, Hahn K, Samann PG, Fahrmeir L, Auer DP. Assessing DTI data quality using bootstrap analysis. Magn Reson Med. 2004; 52(3):582–9. [PubMed: 15334578]
36. Anderson AW. Theoretical analysis of the effects of noise on diffusion tensor imaging. Magn Reson Med. 2001; 46(6):1174–88. [PubMed: 11746585]
37. Chang L-C, Koay CG, Pierpaoli C, Basser PJ. Variance of estimated DTI-derived parameters via first-order perturbation methods. Magnetic Resonance in Medicine. 2007; 57(1):141–149. [PubMed: 17191228]
38. Jones DK. The effect of gradient sampling schemes on measures derived from diffusion tensor MRI: a Monte Carlo study. Magn Reson Med. 2004; 51(4):807–15. [PubMed: 15065255]
39. Skare S, Hedehus M, Moseley ME, Li TQ. Condition number as a measure of noise performance of diffusion tensor data acquisition schemes with MRI. J Magn Reson. 2000; 147(2):340–52. [PubMed: 11097823]
40. Sun SW, Neil JJ, Liang HF, He YY, Schmidt RE, Hsu CY, Song SK. Formalin fixation alters water diffusion coefficient magnitude but not anisotropy in infarcted brain. Magn Reson Med. 2005; 53(6):1447–51. [PubMed: 15906292]
41. D'Arceuil H, de Crespigny A. The effects of brain tissue decomposition on diffusion tensor imaging and tractography. Neuroimage. 2007; 36(1):64–8. [PubMed: 17433879]
42. Rane S, Duong TQ. Comparison of In Vivo and Ex Vivo Diffusion Tensor Imaging in Rhesus Macaques at Short and Long Diffusion Times. The Open Neuroimaging Journal. 2011; 5:172–178. [PubMed: 22253659]
43. McNab JA, Jbabdi S, Deoni SC, Douaud G, Behrens TE, Miller KL. High resolution diffusion-weighted imaging in fixed human brain using diffusion-weighted steady state free precession. Neuroimage. 2009; 46(3):775–85. [PubMed: 19344686]
44. Miller KL, Stagg CJ, Douaud G, Jbabdi S, Smith SM, Behrens TE, Jenkinson M, Chance SA, Esiri MM, Voets NL, et al. Diffusion imaging of whole, post-mortem human brains on a clinical MRI scanner. Neuroimage. 2011; 57(1):167–81. [PubMed: 21473920]

45. Srinivasan M, Sedmak D, Jewell S. Effect of fixatives and tissue processing on the content and integrity of nucleic acids. Am J Pathol. 2002; 161(6):1961–71. [PubMed: 12466110]
46. Oouchi H, Yamada K, Sakai K, Kizu O, Kubota T, Ito H, Nishimura T. Diffusion anisotropy measurement of brain white matter is affected by voxel size: underestimation occurs in areas with crossing fibers. AJNR Am J Neuroradiol. 2007; 28(6):1102–6. [PubMed: 17569968]
47. Schumann CM, Buonocore MH, Amaral DG. Magnetic resonance imaging of the postmortem autistic brain. J Autism Dev Disord. 2001; 31(6):561–8. [PubMed: 11814267]
48. Tovi M, Ericsson A. Measurements of T1 and T2 over time in formalin-fixed human whole-brain specimens. Acta Radiol. 1992; 33(5):400–4. [PubMed: 1389643]
49. Thelwall PE, Shepherd TM, Stanisz GJ, Blackband SJ. Effects of temperature and aldehyde fixation on tissue water diffusion properties, studied in an erythrocyte ghost tissue model. Magn Reson Med. 2006; 56(2):282–9. [PubMed: 16841346]
50. Gao, Y.; Choe, AS.; Li, X.; Stepniewska, I.; Anderson, AW. Comparison of in vivo and ex vivo DTI cortical connectivity measurements in the squirrel monkey brain. Salt Lake City, Utah, USA: 2013.
51. Collins CE, Airey DC, Young NA, Leitch DB, Kaas JH. Neuron densities vary across and within cortical areas in primates. Proc Natl Acad Sci U S A. 2010; 107(36):15927–32. [PubMed: 20798050]
52. Pierpaoli C, Jezzard P, Basser PJ, Barnett A, Chiro GD. Diffusion Tensor MR Imaging of the Human Brain. Radiology. 1996; 201:637–648. [PubMed: 8939209]
53. Cercignani M, Inglese M, Elisabetta Pagani GC, Filippi M. Mean Diffusivity and Fractional Anisotropy Histograms of Patients with Multiple Sclerosis. AJNR Am J Neuroradiol. 2001; 22:952–958. [PubMed: 11337342]
54. Emmer BJ, Grond Jvd, Steup-Beekman GM, Huizinga TWJ, Buchem1 MAv. Selective Involvement of the Amygdala in Systemic Lupus Erythematosus. PLoS Medicine. 2005; 3(12): 2285–2290.
55. Zhang L, Harrison M, Heier LA, Zimmerman RD, Ravdin L, Lockshin M, Ulug AM. Diffusion changes in patients with systemic lupus erythematosus. Magn Reson Imaging. 2007; 25(3):399–405. [PubMed: 17371731]
56. Welsh RC, Rahbar H, Foerster B, Thurnher M, Sundgren PC. Brain diffusivity in patients with neuropsychiatric systemic lupus erythematosus with new acute neurological symptoms. J Magn Reson Imaging. 2007; 26(3):541–51. [PubMed: 17729344]
57. Jones, DK. Diffusion MRI: Theory, Methods, and Applications. Oxford University Press; USA: 2010. p. 322-323.
58. Cloutman LL, Lambon Ralph MA. Connectivity-based structural and functional parcellation of the human cortex using diffusion imaging and tractography. Front Neuroanat. 2012; 6:34. [PubMed: 22952459]
59. Mars RB, Jbabdi S, Sallet J, O'Reilly JX, Croxson PL, Olivier E, et al. Diffusion-weighted imaging tractography-based parcellation of the human parietal cortex and comparison with human and macaque resting-state functional connectivity. J Neurosci. 2011; 31(11):4087–100. [PubMed: 21411650]
60. Tomassini V, Jbabdi S, Klein JC, Behrens TE, Pozzilli C, Matthews PM, et al. Diffusion-weighted imaging tractography-based parcellation of the human lateral premotor cortex identifies dorsal and ventral subregions with anatomical and functional specializations. J Neurosci. 2007; 27(38): 10259–69. [PubMed: 17881532]

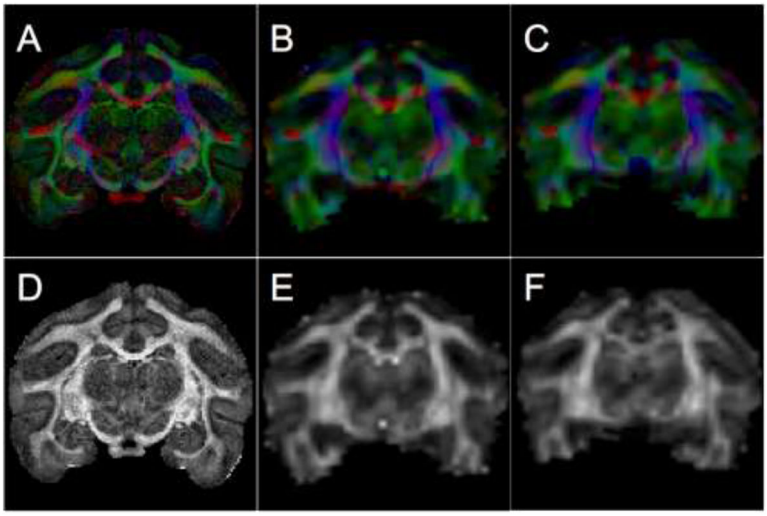

Figure 1.

Color-maps (A–C) and scalar FA maps (D–F) from a coronal slice of the *in vivo* session 1 (A,D), and *in vivo* session 2 (B,E), and ex vivo session (C,F) of the same brain. Color-maps show the orientation of the principal direction of diffusion, with red, green, and blue representing diffusion along medial-lateral, anterior-posterior, and superior-inferior directions, respectively. The color intensity is proportional to the FA.

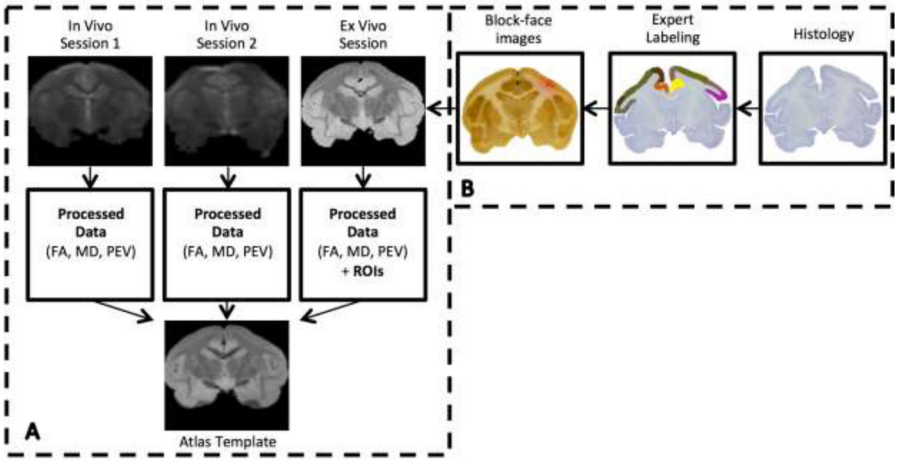

Figure 2.

Data processing pipeline. Registration of *in vivo* and *ex vivo* scans to a common space (A), and definition of ROI and registration to MRI space (B).

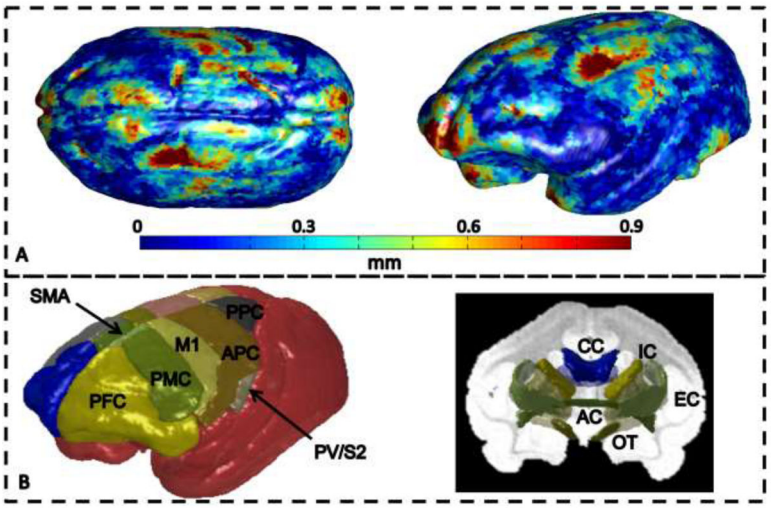

Figure 3.

Registration quality metric over the surface of the template image averaged over all animals (A), and 3D ROIs for GM regions (left) and WM tracts (right) for one monkey (B). In (B) GM ROIs are labeled on left brain hemisphere reconstructed from cortical sections and include: prefrontal cortex, PFC; premotor cortex, PMC; primary motor cortex, M1; supplementary motor area, SMA; anterior cingulate cortex, ACC (not visible on dorsolateral view of brain); anterior parietal cortex, APC, includes somatosensory areas 3b,1–2 and possibly adjacent parts of posterior parietal cortex; parietal ventral and secondary somatosensory areas, PV/S2, within the dorsal bank of lateral sulcus; posterior parietal cortex, PPC; and primary visual cortex, V1, not visible. WM ROIs include: corpus callosum (CC), internal capsule (IC), external capsule (EC), anterior commissure (AC), and optic tract (OT).

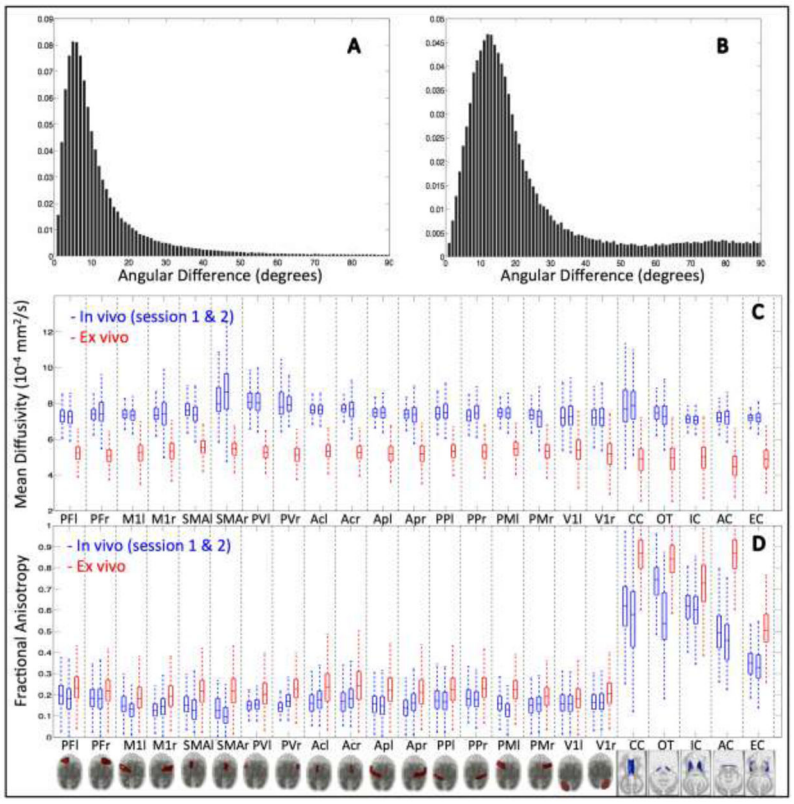

Figure 4.

Voxel-wise and ROI-based comparisons of PEV, MD, and FA. The angular difference in primary eigenvectors over all white matter voxels is shown for two *in vivo* scans (A), and for *in vivo* scan session 1 versus the *ex vivo* scan session (B). *In vivo* and *ex vivo* comparisons of MD (C) and FA (D), across all ROIs for both *in vivo* (blue) and *ex vivo* (red) scan sessions. “r” and “l” designate anatomic right and left, respectively.

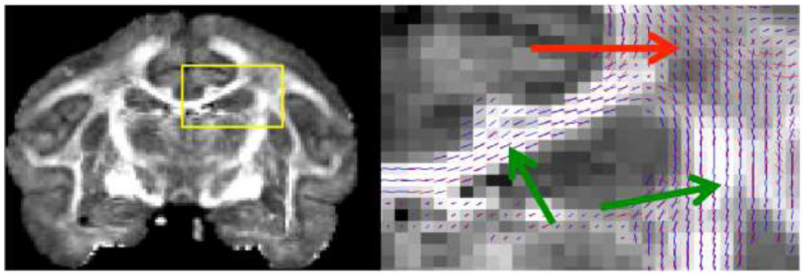

Figure 5.

Voxel-wise comparison of *in vivo* and *ex vivo* PEV orientation. Coronal *ex vivo* FA map (left) with insert (yellow frame) enlarged to show location of white matter region (right) which includes lines of principal eigenvector of *ex vivo* (red) and *in vivo* (blue) sessions of a single monkey. Green arrow points towards regions of high agreement (corpus collosum, corticospinal tract), and red arrow points towards region of crossing fibers and low agreement.

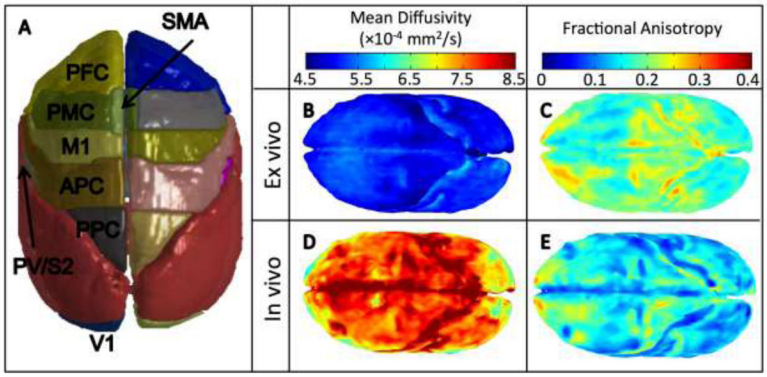

Figure 6.

Diffusion measures across the *in vivo* and *ex vivo* squirrel monkey cortex, averaged across animals. 3D rendering of gray matter ROIs (A), and voxel-wise renderings of MD (B,D) and FA (C,E) across the cortex.

Table 1

In vivo values for mean MD and FA within GM and WM ROIs, and intra-subject and inter-subject variability of mean MD and mean FA.

		Mean Diffusivity			Fractional Anisotropy		
ROI	**ROI SNR**	**Mean Across Subjects (Grand Mean)**	**Mean Intra-subject CV (%)**	**Inter-subject CV(%)-based on mean across sessions**	**Mean Across Subjects (Grand Mean)**	**Mean Intra-subject CV (%)**	**Inter-subject CV(%)-based on mean across sessions**
PFl	~32	7.02	6.87	3.49	0.23	8.12	21.46
PFr		7.27	4.47	2.42	0.22	4.85	19.29
M1l		7.54	1.77	5.04	0.19	16.81	24.76
M1r		7.57	0.86	3.68	0.17	9.46	20.53
SMAl		7.89	3.48	4.72	0.18	8.09	24.84
SMAr		8.25	2.16	2.09	0.17	8.31	30.60
PVl		7.99	2.62	2.82	0.19	9.76	18.53
PVr		8.07	2.89	1.50	0.18	7.71	9.21
ACl		7.98	1.32	4.35	0.21	8.13	18.84
ACr		8.01	2.18	3.85	0.21	8.00	17.27
APl		7.54	2.75	0.38	0.21	10.25	27.43
APr		7.73	2.24	5.29	0.19	9.78	17.42
PPl		7.75	1.61	1.59	0.23	14.61	31.48
PPr		7.95	5.08	7.50	0.21	5.59	9.99
PMl		7.41	2.61	2.20	0.19	10.40	22.76
PMr		7.45	2.37	3.58	0.18	6.50	16.04
V1l		7.42	2.04	1.29	0.18	13.54	13.01
V1r		7.35	1.48	0.91	0.19	8.97	10.88
CC	~21	7.89	4.45	1.71	0.64	7.81	11.46
OC		7.44	2.61	0.67	0.70	8.37	7.31
IC		7.13	0.36	0.60	0.61	1.55	3.43
ANC		7.20	2.55	4.24	0.55	4.08	12.67
EC		7.21	0.43	1.98	0.38	2.15	11.06